Fault detection through monitoring of the AC variables in Grid Connected PV systems

Nikolaos SAPOUNTZOGLOU and Bertrand RAISON
Univ. Grenoble Alpes, CNRS, Grenoble INP*, G2Elab, 38000 Grenoble, France

ABSTRACT – A fault detection algorithm for grid-connected photovoltaic (GCPV) systems is presented in this paper. After a synthetic description of the most important fault detection techniques up to date, the selection of the signal approach and of the output of the inverter as a measurement point for the monitored electrical variables, for this study, are explained. In Section 2, the procedure that was followed to build a GCPV model is discussed. In Section 3, the different sources of faults that were studied are presented and the necessary steps to construct the fault signature table are demonstrated. In Section 4, the developed algorithm and its threshold crossing parameters are analyzed. The algorithm is able to identify the different types of faults or groups of them in less than 100 ms under the assumption that only one fault is occurring at a time. Finally, the robustness of the algorithm for various irradiance levels was validated via simulations.

Keywords – Fault detection, PV modeling, GCPV system

1. INTRODUCTION

The integration of renewable energy sources in the grid is constantly growing with PVs playing an important role. In France, the installed capacity of GCPVs by the end of September 2017 was 7,239 $[MW]$ accounting for 1.9% of the consumed electricity [1]. At the same time, society's dependence on electricity is rapidly rising, rendering the need to mitigate the economic and social impact of electricity interruptions necessary. Therefore, a fault should be detected, located and isolated as quickly as possible.

Over the last years, numerous fault detection and isolation techniques have been developed for GCPVs [2]-[14]. The most popular fault detection techniques for GCPVs are the ones that rely on simple comparisons between the measured values of the electrical variables such as the current, the voltage or the power and their values from simulations. These comparisons usually require atmospheric data as input, such as the irradiance level and the cell's temperature [2, 3]. Another common detection method is based on monitoring the changes of I-V curves of the PV modules and strings [4, 5]. In addition to these methods, statistical approaches were investigated in [6, 7]. Furthermore, neural networks [8] and fuzzy logic [9] methods were used by some researchers to detect PV faults. Other methods ranging from infrared thermography [10] to time domain reflectometry [11] and satellite irradiance measurements [12], although being uncommon, they provide interesting results. Finally, signal analysis methods were investigated in [13, 14].

However, most of these studies examined a limited amount of fault cases [2, 3, 5, 6, 7, 8, 12, 14], others have proven to be quite costly [4, 12] and others were based on a very specific set of training data [8, 9]. Until now, most of the research was focused on a specific source of faults, mainly the PV array and in some cases the inverter. Moreover, there has been no study so far where only the ac electrical variables were used to detect faults on the dc side of the GCPV.

This study explores a different approach. Its main objective is to detect faults occurring on the dc side of the plant via the monitoring of electrical variables on the ac side which will result in the use of fewer sensors and thus reducing the cost of the installation. For this purpose and among the various available topologies, the common two-stage conversion topology was selected to connect the PV system to the electrical grid through a three phase connection.

The development of this model is discussed in the next Section followed by an analysis of the fault cases under study and the construction of the fault signature table in Section 3. Section 4 provides a thorough insight of the proposed algorithm and describes the configuration of the threshold crossing settings. This paper concludes with a summary of the effectiveness of the algorithm and the possibilities of further extending this work.

2. MODELING OF A PV SYSTEM

Modeling a PV array is a challenging and complicated task. There are three basic steps in order to design a model of a PV array : 1) extraction of the basic parameters from the equations describing the equivalent circuit of a PV cell, using only the available data from the manufacturer's datasheet, 2) usage of the known parameters to solve the transcendental current-voltage characteristic equation and 3) synthesis of several elements in series and in parallel to construct the PV array [15].

2.1. PV Cell : Bishop's model

Although the one-diode model is used in numerous research projects, it does not take into consideration the avalanche effect of the diode [16]. But studying a PV cell under a fault, demands monitoring of the cell's activity in the first (I), second (II) and fourth (IV) quadrant of the I-V characteristic curve as shown in Fig. 1a. That is achieved by using Bishop's model, whose equivalent circuit is presented in Fig 1b.

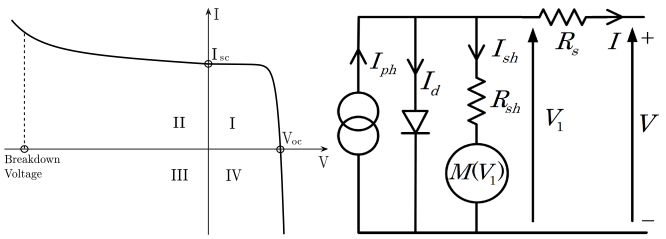

(a) I-V characteristic curve (b) Equivalent circuit

Fig. 1. Bishop's model [16]

The Bishop's model is an upgraded version of the one-diode model with a non-linear multiplication factor added in series with the shunt resistance. The mathematical equation describing the model is given in (1).

*Institute of Engineering Univ. Grenoble Alpes

$$I = I_{ph} - I_0 \cdot \left[exp\left(\frac{V + R_s \cdot I}{V_t} \right) - 1 \right] - \frac{V + R_s \cdot I}{R_{sh}} \cdot \left[1 + k \cdot \left(1 - \frac{V + R_s \cdot I}{V_b} \right)^{-n} \right] \quad (1)$$

Eight parameters can be distinguished from (1). Those parameters are : the photo current I_{ph}, the diode reverse saturation current I_o, the diode's thermal voltage V_t, the series resistance R_s, the shunt resistance R_{sh}, the Bishop's coefficients k ($\sim$0.1) and n (3.4-4) and the breakdown voltage V_b. Since (1) is a transcendental equation, a numerical solution is obligatory. In this study, the Newton-Raphson algorithm [17] was used to solve the equation, although the Lambert-W function could be an alternative solution [18].

Table 1. PV system characteristics at standard test conditions (STC) [19]

Parameter	Symbol	Value	Unit
Photo current	I_{ph}	4.838	$[A]$
Reverse diode saturation current	I_o	10^{-7}	$[A]$
Thermal voltage	V_t	0.0257	$[V]$
Series resistance	R_s	0.005	$[\Omega]$
Shunt resitance	R_{sh}	9	$[\Omega]$
Bishop's coefficient	k	0.1	–
Bishop's coefficient	n	3.4	–
Breakdown voltage	V_b	-30	$[V]$
Number of cells per module	N_{cell}	72	–
Number of modules per string	N_{mod}	10	–
Number of strings	N_{str}	30	–
Number of bypass diodes per module	N_{bpd}	4	–
Short circuit current	I_{sc}	145.3	$[A]$
Open circuit voltage	V_{oc}	407.67	$[V]$
Output power	P_{pv}	43.2	$[kW]$
Dc bus capacitance	C_{bus}	6	$[mF]$
Grid inductance	L_{grid}	5	$[mH]$
Grid resistance	R_{grid}	5	$[m\Omega]$
Grid frequency	f_{grid}	50	$[Hz]$
Gird voltage	$V_{LL_{grid_{rms}}}$	400	$[V]$

2.2. *PV Array*

The creation of the PV array is achieved through the connection, either in series or in parallel, of several PV cells. Here, 72 cells are connected in series to form a string and at the same time strings are connected in parallel to complete the creation of the PV array. Finally, in order to ensure the protection of the PV array, bypass and blocking diodes are used to protect the array against inverse polarization and the flow of inverse currents respectively. In this study, a PV system of 43.2 $[kW]$ output power was used as a basis for the simulations.

2.3. *PV System*

The PV array is connected to the grid through a dc-dc boost converter and an inverter as shown in Fig. 2. The exact models of the power electronics devices were used to run the simulations. All the parameters of the designed GCPV system can be found in Table 1 ; the values of the parameters are given for stantard test conditions (STC) of 1000 $[W/m^2]$ and 25 $[^oC]$.

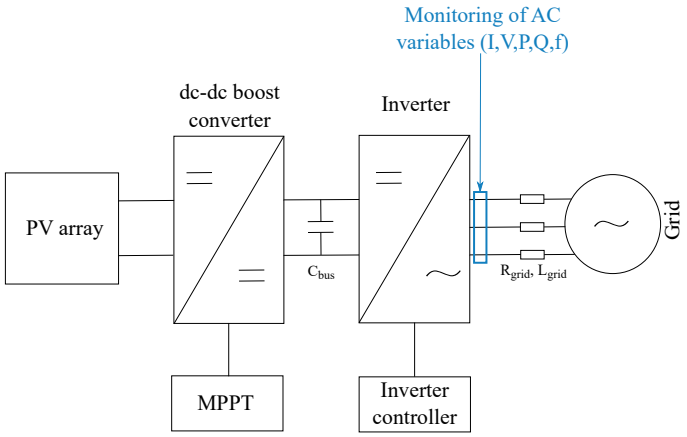

Fig. 2. PV system schematic

3. FAULT DETECTION

As explained in the Introduction, the objective of this work is to detect and identify the fault and its location by monitoring the ac electrical variables. The measurement point, presented in Fig. 2, is located at the output of the inverter. The monitored electrical variables were the following : the current (I), the voltage (V), the active power (P), the reactive power (Q) and the frequency (f) which was obtained from the measured voltage via a phase locked loop.

3.1. *Fault types*

Four different parts of the PV system were considered as point of origin of faults in this study : the PV array itself where shading and diode faults were studied, the dc bus and the two power electronics devices : the boost converter and the inverter, where the switching devices, in this case insulated-gate bipolar transistos (IGBTs), were under a short-circuit (SC) or open-circuit (OC) fault. A detailed list of the examined faults is presented below :

a) PV array faults :
   [f01] shading of a number of PV modules
   [f02] inverse bypass diode
   [f03] short-circuited bypass diode
   [f04] bypass diode breakdown

b) converter faults :
   [f05] boost converter IGBT on OC
   [f06] boost converter IGBT on SC

c) dc bus faults :
   [f07] SC between the positive pole and the ground
   [f08] SC between the negative pole and the ground

d) inverter faults :
   [f09] inverter IGBT OC (1 IGBT in 1 leg)
   [f10] inverter full leg OC (all IGBTs in 1 leg)
   [f11] inverter IGBT SC (1 IGBT in 1 leg)
   [f12] inverter full leg SC (all IGBTs in 1 leg)

More precisely, for the simulation of the shaded PV modules fault, a shade covering the 30% of the surface of the first five modules in the first twenty out of a total of thirty strings was applied through a reduction of their photocurrent by 30%. Additionally, in order to simulate the diode breakdown fault, a resistance of 5 [Ω] was used to replace the diode.

3.2. *Fault signature*

The first set of analyses investigated the impact of the occurrence of the different types of faults on the monitored electrical variables (I, V, P, Q and f). The results were gathered in Table 2 where "1" signifies a change in the value of the variable after

the fault occurrence while "0" the fact that the variable remains unaffected. An obvious observation from Table 2, is that three of the five variables were affected in every fault case : the current, the active and the reactive power. Hence, it was decided that a change in the active power is a strong indicator of a fault occurrence under the assumption that the irradiance has not changed. In order to calculate the estimated active power output of the PV system, a real time irradiance measurement is necessary. This is generally accomplished through the use of calibrated PV reference devices [20]. With the irradiance measurements available, the estimation of the active power becomes attainable and thus the detection of a fault is achieved through a comparison of the value of the measured active power and the estimated one based on the irradiance level.

Table 2. Monitored variables

Faults	Changes in variables				
	ΔI	ΔV	ΔP	ΔQ	Δf
f01	1	0	1	1	0
f02	1	0	1	1	0
f03	1	0	1	1	0
f04	1	0	1	1	0
f05	1	1	1	1	0
f06	1	1	1	1	0
f07	1	1	1	1	0
f08	1	1	1	1	0
f09	1	1	1	1	1
f10	1	1	1	1	1
f11	1	1	1	1	1
f12	1	1	1	1	1

However, from Table 2 only fault categories can be discriminated and not individual fault cases. For this purpose and in order to obtain a unique fault signature for each fault case, six symptoms were generated. First of all, the equality to zero of the sum of the phase currents was examined (s1). Secondly, the number of the phases where the current during faulty operation (FO) was zero, was also recorded (s2). Then the behaviors of the current and the voltage in each phase were monitored and the results were compared to their values during normal operation (NO). Thus, the indices of $\Delta I = I_{FO} - I_{NO}$ and $\Delta V = V_{FO} - V_{NO}$ were created. From those indices, two additional symptoms were created : the per phase increase or decrease of the current (s3) and the number of phases where the voltage decreases after the fault occurrence (s4). Finally, two more symptoms were generated by monitoring the frequency components of the measured voltage. The two indicators of a fault occurrence in this case were the absence of the 10 $[kHz]$ (s5) and 50 $[Hz]$ (s6) frequency components of the voltage. The complete list of symptoms is provided below :

- **[s1]** the sum of phase currents is equal to zero, $\sum i = 0$
- **[s2]** in how many of the three phases is $I_{FO} = 0$
- **[s3]** current increase $\Delta I > 0$ or current decrease $\Delta I < 0$
- **[s4]** in how many of the three phases is $\Delta V < 0$
- **[s5]** absence of the 10 $[kHz]$ frequency component of the voltage
- **[s6]** absence of the 50 $[Hz]$ frequency component of the voltage

Based on these symptoms the fault signature table, Table 3, was created. For symptoms s1, s5 and s6 the "$\surd$" symbol is used to mark an affirmative answer to the posed question while "x" is used to mark a negative response. For s1 specifically, "$+$" and "$-$" indicate the sign of the sum of the phase currents. Similarly, for s3, "$-$" means that the current during faulty operation has a smaller value than normal operation and "$+-$" that the current is in some phases greater $(+)$ than the one in normal operation and smaller $(-)$ in the rest. Finally, for symptoms s2 and s4 the numbers "0-3" signify the number of phases affected by the criterion of each symptom.

Table 3. Fault signature table

Faults	Symptoms					
	$s1$	$s2$	$s3$	$s4$	$s5$	$s6$
f01	$\surd$	0	$-$	0	x	x
f02	$\surd$	0	$-$	0	x	x
f03	$\surd$	0	$-$	0	x	x
f04	$\surd$	0	$-$	0	x	x
f05	$\surd$	3	$-$	3	x	x
f06	$\surd$	3	$-$	3	x	x
f07	$-$	0	$-$	3	$\surd$	$\surd$
f08	$+$	0	$-$	3	$\surd$	$\surd$
f09	$\surd$	0	$+-$	0	x	x
f10	$\surd$	1	$+-$	1	$\surd$	x
f11	$\surd$	0	$+-$	3	x	x
f12	$\surd$	0	$+-$	3	$\surd$	$\surd$

A first conclusion from Table 3 is that out of the twelve different fault cases, six faults and two groups of faults can be identified. The first group of faults consists of all the faults inside the PV array (f01-f04), an expected result since the point of origin of the fault is far from the measurement point (at the output of the inverter). For the same reason, faults inside the converter (f05-f06) can only be identified as a group of faults since they present an identical fault signature as well. The rest of the fault cases (f07-f12), faults on the dc bus and inside the inverter, can all be uniquely identified as they all have different fault signatures.

4. FAULT LOCALIZATION

As it was mentioned in the previous Section, a fault can be detected through a change in the value of the active power. For the localization of the faults however, a localization algorithm was developed based on the fault signature table. The algorithm is able to identify the previously described different fault cases and group of faults and create an alarm signal in less than 100 $[ms]$.

4.1. Fault localization algorithm

In Fig. 5 the flowchart of the algorithm is presented. The algorithm initiates when the measured active power at the inverter output is different from the estimated one for the current irradiance level. The first symptoms to be checked were the s1 and s2. If the sum of the phase currents was not equal to zero (s1) and if on top of that the sum was positive, then the negative pole to ground SC fault (f08) on the dc bus was identified. If however, the sum of the currents was negative, then the positive pole to ground SC fault (f07) was identified.

Following the right branch of the flowchart, the symptoms s2,

s3 and s4 were used consecutively to identify a series of faults. The first one to be checked was s2 and in how many phases the current was zero. If it was zero in all three phases then the category of boost faults (f05, f06) was identified. On the other hand, if the current was not zero in any of the phases the next criterion was used, s3. There, if the current during faulty operation was smaller than the one in normal operation in all three phases, then the group of PV faults (f01-f04) was found. Furthermore, if the current difference was positive in some phases and negative in others, then the algorithm proceeded to next step where the s4 was checked. Moreover, if no voltage drop was noticed during faulty operation in any of the phases, then the identified fault was the OC of one IGBT in one of the legs of the inverter (f09).

Returning back to the case where the sum of phase currents is equal to zero (s1) and following the "yes" branch of this decision block, if both the frequency components of the voltage at 10 $[kHz]$ and 50 $[Hz]$ dissapeared after the fault occurrence, then the identified fault case was the SC of both IGBTs in one of the inverter legs. On the contrary, if the frequency component of the voltage at 50 $[Hz]$ was not zero and if at the same time a voltage drop was noticed in all three phases, then the SC of one of the IGBTs in one of the inverter legs was identified. In this case, it was also possible to identify the faulty IGBT by checking the behavior of the voltage in each phase (close to zero with some spikes on the faulty phase). Finally, the last fault to be identified was the OC of both of the IGBTs in one of the inverter legs. Again, the detection of the faulty phase was possible since the current of the phase under fault was equal to zero.

4.2. *Configuration of threshold crossing settings*

For the implementation of the localization algorithm, the environment of MATLAB/Simulink was used. The configuration of the threshold crossing settings was adjusted in such a way so that the algorithm would perform accurately for all the tested irradiance levels (1000, 800, 600, 400 and 200 $[W/m^2]$).

Beginning with s1, the instantaneous values of the currents were added in order to trace their sum. Continuing with s2, the rms value of the current was monitored. For both s1 and s2 the equality to zero was verified through the implementation of a threshold of 1 $[A]$ around zero ($-1[A] < I < 1[A]$) which corresponded to 1% of the nominal value of the current at STC.

Passing on to the s3 and s4 symptoms the difference of the monitored variables (I, V) between faulty and normal operation was created based on their moving maximum values over a sliding window of 40 $[ms]$ (equal to twice the period of the signal, 20 $[ms]$) in order to attain their maximum values at all times. The negative value of ΔV was defined as lower than 5 $[V]$ (1% of V_{NO} at STC) while the current settings, in order to avoid any false detection at low irradiance levels under 400 $[W/m^2]$, were designed around 2 $[A]$ (2% of I_{NO}).

For the threshold settings of the frequency components of the voltage, a bandpass filter and a lowpass filter were used for 10 $[kHz]$ and 50 $[Hz]$ respectively. The equality to zero of their output was checked with a threshold crossing around 5 $[V]$, $-5[V] < V_{f50}, V_{f10k} < 5[V]$, which again corresponded to 1% of V_{NO} at STC. This disappearance of the voltage frequency components is visible in the spectrograms presented in Fig. 3 and Fig. 4 for the 10 $[kHz]$ and 50 $[Hz]$ cases respectively; the example of f12 is used to demonstrate the changes in the frequency components. In both cases after the fault occurrence at 0.5 $[s]$, a sudden drop of the filters's outputs is noticed (marked by a color change in the dBm scale).

4.3. *Algorithm validation*

The robustness of the algorithm was validated via simulations in the Simulink environment for the same irradiance levels that were used for the extraction of data and the configuration of the threshold settings (1000, 800, 600, 400 and 200 $[W/m^2]$). As it was mentioned before, the algorithm detects and localizes the faults in less than 100 $[ms]$; in 10.51 $[ms]$ in the best case scenario and in 96.93 $[ms]$ in the worst case scenario. More analytically, the fault detection times for each localizable fault case are presented in Table 4.

5. CONCLUSIONS

In this paper, a fault detection algorithm for GCPV systems was presented, able to detect and localize six faults and two groups of faults under the assumption that only one fault is occurring at a time. Twelve common faults throughout the PV system were considered in this study. The algorithm creates an alarm signal in less than 100 $[ms]$. Its robustness was validated

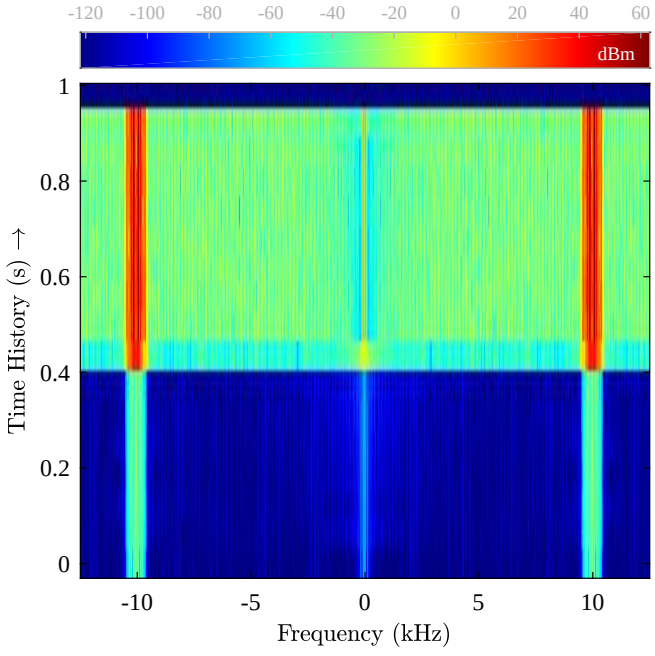

Fig. 3. Spectrogram of the bandpass filter's output around 10 $[kHz]$ (s5) for the full leg SC fault case (f12)

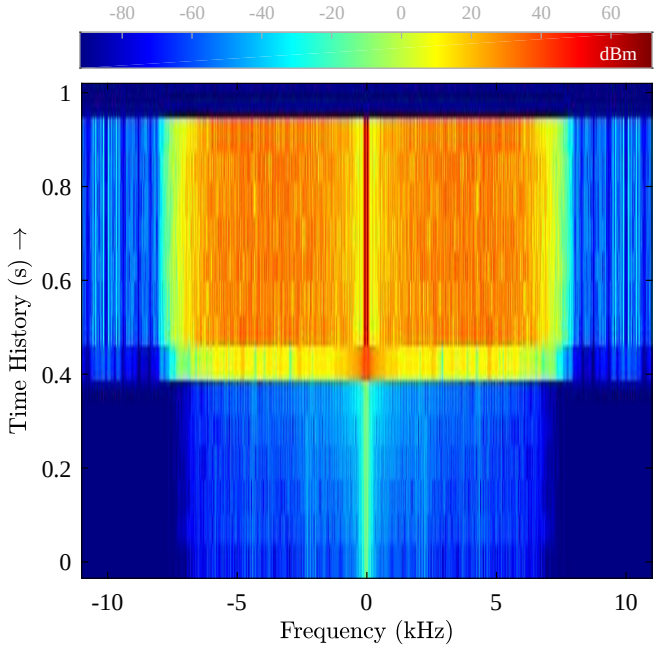

Fig. 4. Spectrogram of the lowpass filter's output around 50 $[Hz]$ (s6) for the full leg SC fault case (f12)

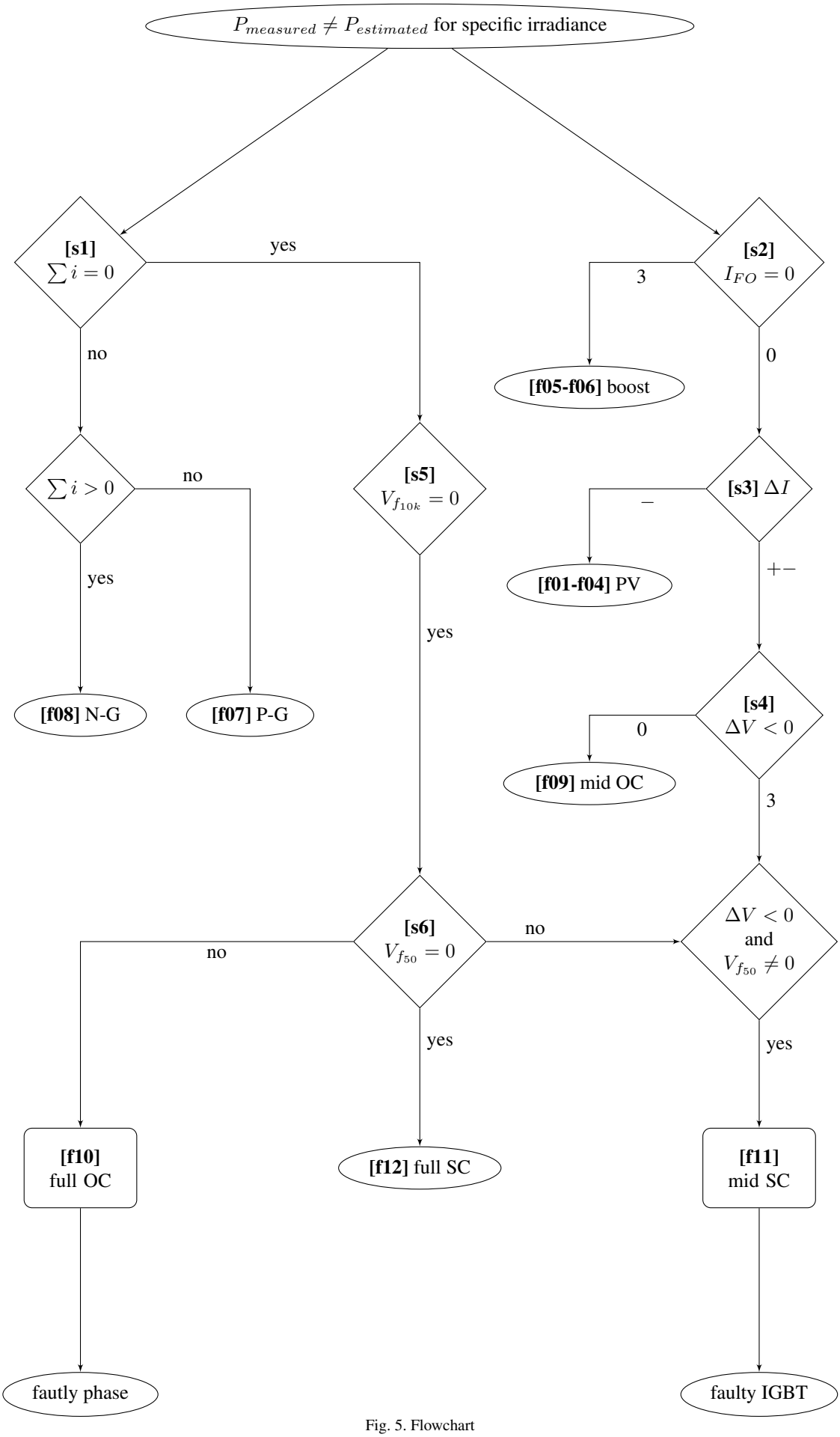

Fig. 5. Flowchart

Table 4. Fault detection times

Faults	$min(t_{det})[ms]$	$max(t_{det})[ms]$
f01-04	25.04	36.74
f05-06	14.20	19.85
f07	24.35	24.39
f08	23.98	24.06
f09	10.51	12.60
f10	42.53	96.93
f11	55.49	59.99
f12	24.34	25.14
global	10.51	96.93

for different irradiance levels via simulations. Further research could be done to increase the number of studied faults and to experimentally validate the algorithm's response.

6. ACKNOWLEDGEMENTS

This project has received funding from the European Union's Horizon 2020 research and innovation programme under the Marie Skłodowska-Curie grant agreement No 675318 (INCITE).

7. REFERENCES

[1] "Panorama de l'électricité renouvelable au 30 Septembre 2017," Tech. Rep. RTE France. [Online]. Available : https://www.rte-france.com/sites/default/files/panorama_09-17-web.pdf

[2] A. Chouder and S. Silvestre, "Automatic supervision and fault detection of PV systems based on power losses analysis," *Energy Conversion and Management*, vol. 51, no. 10, pp. 1929–1937, Oct. 2010. [Online]. Available : http://linkinghub.elsevier.com/retrieve/pii/S0196890410000919

[3] N. Gokmen, E. Karatepe, B. Celik, and S. Silvestre, "Simple diagnostic approach for determining of faulted PV modules in string based PV arrays," *Solar Energy*, vol. 86, no. 11, pp. 3364–3377, Nov. 2012. [Online]. Available : http://linkinghub.elsevier.com/retrieve/pii/S0038092X12003313

[4] J. E. Quiroz, J. S. Stein, C. K. Carmignani, and K. Gillispie, "In-situ module-level I-V tracers for novel PV monitoring," in *2015 IEEE 42nd Photovoltaic Specialist Conference (PVSC)*, Jun. 2015, pp. 1–6.

[5] Y. Hu, J. Zhang, W. Cao, J. Wu, G. Y. Tian, S. J. Finney, and J. L. Kirtley, "Online Two-Section PV Array Fault Diagnosis With Optimized Voltage Sensor Locations," *IEEE Transactions on Industrial Electronics*, vol. 62, no. 11, pp. 7237–7246, Nov. 2015.

[6] M. Dhimish, V. Holmes, and M. Dales, "Parallel fault detection algorithm for grid-connected photovoltaic plants," *Renewable Energy*, vol. 113, no. Supplement C, pp. 94–111, Dec. 2017. [Online]. Available : http://www.sciencedirect.com/science/article/pii/S0960148117304780

[7] E. Garoudja, F. Harrou, Y. Sun, K. Kara, A. Chouder, and S. Silvestre, "Statistical fault detection in photovoltaic systems," *Solar Energy*, vol. 150, pp. 485–499, Jul. 2017. [Online]. Available : http://linkinghub.elsevier.com/retrieve/pii/S0038092X17303377

[8] C. B. Jones, J. S. Stein, S. Gonzalez, and B. H. King, "Photovoltaic system fault detection and diagnostics using Laterally Primed Adaptive Resonance Theory neural network," in *2015 IEEE 42nd Photovoltaic Specialist Conference (PVSC)*, Jun. 2015, pp. 1–6.

[9] P. Ducange, M. Fazzolari, B. Lazzerini, and F. Marcelloni, "An intelligent system for detecting faults in photovoltaic fields," in *2011 11th International Conference on Intelligent Systems Design and Applications*, Nov. 2011, pp. 1341–1346.

[10] N. Gokmen, E. Karatepe, S. Silvestre, B. Celik, and P. Ortega, "An efficient fault diagnosis method for PV systems based on operating voltage-window," *Energy Conversion and Management*, vol. 73, pp. 350–360, Sep. 2013. [Online]. Available : http://linkinghub.elsevier.com/retrieve/pii/S0196890413002744

[11] T. Takashima, J. Yamaguchi, and M. Ishida, "Fault detection by signal response in PV module strings," in *2008 33rd IEEE Photovoltaic Specialists Conference*, May 2008, pp. 1–5.

[12] A. Drews, A. de Keizer, H. Beyer, E. Lorenz, J. Betcke, W. van Sark, W. Heydenreich, E. Wiemken, S. Stettler, P. Toggweiler, S. Bofinger, M. Schneider, G. Heilscher, and D. Heinemann, "Monitoring and remote failure detection of grid-connected PV systems based on satellite observations," *Solar Energy*, vol. 81, no. 4, pp. 548–564, Apr. 2007. [Online]. Available : http://linkinghub.elsevier.com/retrieve/pii/S0038092X06002040

[13] M. González, B. Raison, S. Bacha, and L. Bun, "Fault diagnosis in a grid-connected photovoltaic system by applying a signal approach," in *IECON 2011 - 37th Annual Conference of the IEEE Industrial Electronics Society*, Nov. 2011, pp. 1354–1359.

[14] I. S. Kim, "Fault detection algorithm of the photovoltaic system using wavelet transform," in *India International Conference on Power Electronics 2010 (IICPE2010)*, Jan. 2011, pp. 1–6.

[15] W. De Soto, S. A. Klein, and W. A. Beckman, "Improvement and validation of a model for photovoltaic array performance," *Solar Energy*, vol. 80, no. 1, pp. 78–88, Jan. 2006. [Online]. Available : //www.sciencedirect.com/science/article/pii/S0038092X05002410

[16] L. Bun, B. Raison, G. Rostaing, S. Bacha, A. Rumeau, and A. Labonne, "Development of a real time photovoltaic simulator in normal and abnormal operations," in *IECON 2011 - 37th Annual Conference of the IEEE Industrial Electronics Society*, Nov. 2011, pp. 867–872.

[17] D. Picault, B. Raison, S. Bacha, J. de la Casa, and J. Aguilera, "Forecasting photovoltaic array power production subject to mismatch losses," *Solar Energy*, vol. 84, no. 7, pp. 1301–1309, 2010. [Online]. Available : http://www.sciencedirect.com/science/article/pii/S0038092X10001556

[18] E. I. Batzelis and S. A. Papathanassiou, "A Method for the Analytical Extraction of the Single-Diode PV Model Parameters," *IEEE Transactions on Sustainable Energy*, vol. 7, no. 2, pp. 504–512, Apr. 2016.

[19] L. Bun, "Détection et localisation de défauts pour un systéme PV," PhD Thesis, Université Grenoble Alpes, Nov. 2011. [Online]. Available : https://tel.archives-ouvertes.fr/tel-00647189/document

[20] L. Dunn, M. Gostein, and K. Emery, "Comparison of pyranometers vs. PV reference cells for evaluation of PV array performance," in *2012 38th IEEE Photovoltaic Specialists Conference*, Jun. 2012, pp. 002 899–002 904.